APS physics

CHORUS

This is the accepted manuscript made available via CHORUS. The article has been published as:

Field-induced metastability of the modulation wave vector in a magnetic soliton lattice

M. Zhu, J. Peng, T. Hong, K. Prokes, T. Zou, Z. Q. Mao, and X. Ke

Phys. Rev. B **95**, 134429 — Published 19 April 2017

DOI: 10.1103/PhysRevB.95.134429

Field-induced metastability of modulation wave vector in a magnetic soliton lattice

M. Zhu[1], J. Peng[2], T. Hong[3], K. Prokes[4], T. Zou[1], Z. Q. Mao[5], X. Ke[1*]

[1]*Department of Physics and Astronomy, Michigan State University, East Lansing, Michigan 48824, USA*

[2]*Collaborative Innovation Center of Advanced Microstructures, Lab of Solid State Microstructures, School of Physics, Nanjing University, Nanjing 210093, People's Republic of China*

[3]*Quantum Condensed Matter Division, Oak Ridge National Laboratory, Oak Ridge, Tennessee 37831, USA*

[4]*Helmholtz-Zentrum Berlin fur Materialien und Energie, Hahn-Meitner Platz 1, D-14109, Berlin, Germany*

[5]*Department of Physics and Engineering Physics, Tulane University, New Orleans, Louisiana 70118, USA*

*Correspondence to: ke@pa.msu.edu.

We present magnetic-field-induced metastability of the magnetic soliton lattice in a bilayer ruthenate $Ca_3(Ru_{1-x}Fe_x)_2O_7$ (x = 0.05) through single-crystal neutron diffraction study. We show that the incommensurability of the modulation wave vector at zero field strongly depends on the history of magnetic field at low temperature, and that the equilibrium ground state can be achieved by warming above a characteristic temperature $T_g \sim 37$ K. We suggest that such metastability might be associated with the domain wall pinning by the magnetic Fe dopants.

Metastable states, which often emerge when the phase transformation to the thermodynamic equilibrium state is kinetically prohibited, have been commonly observed in nature. The supercooling and superheating phases associated with first-order transitions are prototypical examples [1]. Metastable states can have extended lifetime and can be created via different routes, for instance, by means of rapid cooling [2], or in phase transitions occurring at low temperature such that thermal fluctuations are not sufficiently strong to overcome the intervening energy barriers in the free energy landscape. In the latter case the kinetics of the phase transition is arrested and thus rapid cooling is not necessary. Typical examples include the field-induced magnetic transitions in phase-separated manganites [3,4,5,6] and the field-induced metastable vortex lattices in superconducting MgB_2 [7,8].

Recently, magnetic materials with modulated incommensurate (ICM) spin structures have reignited intense interest owing to their potential of being the multiferroic candidates [12,13]. The uniformly modulated magnetic structures can be distorted by the magnetocrystalline anisotropy and evolve into a magnetic soliton lattice, i.e., nearly commensurate (CM) structures separated by periodic domain walls (solitons) [14], which has been observed in a variety of materials [15,16,17,18,19,20,21]. In general, materials can undergo ICM-CM magnetic phase transitions by varying temperature, magnetic field or pressure. Of particular interest is that, when the ICM-CM magnetic transition is driven by non-thermal control parameters at low temperature, sometimes the system cannot restore the original equilibrium state but instead gets trapped in a metastable phase, leading to irreversibility in the magnetic phase transition. One example of such metastability is the pressure dependence of the modulation wave vector of the spin density wave ordering in metallic Cr, where the system is locked into the high-pressure state at low temperature after the pressure has been released [22]. Similar irreversibility features have also

been reported in the magnetic-field-induced transitions in $NaFe(WO_4)_2$ [23] and $Ba_{0.5}Sr_{1.5}Zn_2(Fe_{1-x}Al_x)_{12}O_{22}$ [24], where the high-field magnetic wave vector is maintained as the magnetic field decreases, and in $TbMnO_3$ [25], $DyMn_2O_5$ [26], UNiAl [27], where the propagation vectors of the low-field magnetic structures as the magnetic field sweeps down are different from either the high-field state or the initial low-field phases after zero-field-cooling. A common feature among these irreversible magnetic transitions is that the magnetic history effect can be erased by warming up above the transition temperature, suggesting that thermal fluctuations are essential in the emergence of such metastability.

In this paper, we present the magnetic-field-induced metastability of the magnetic soliton lattice phase observed in the bilayer ruthenate $Ca_3(Ru_{1-x}Fe_x)_2O_7$ (x = 0.05), which gives rise to irreversibility in the modulation wave vector in the ICM-CM magnetic phase transition. Such a feature is distinct from the reversible phase transitions that have been commonly seen, i.e., the initial and final states are the same before and after varying the control parameter. In addition, we show that the ordering wave vector of Fe-doped $Ca_3Ru_2O_7$ at zero field after field sweeping is different from that in either the high-field state or the initial low-field phase, which strongly depends on the history of the magnetic field and temperature. Furthermore, this metastable state persists below a characteristic temperature $T_g \sim 37$ K above which the equilibrium ground state is restored, indicating that thermal fluctuations play a key role. We suggest that the observed metastability is attributable to the interaction between the magnetic domain walls and the dilute magnetic Fe dopants.

The parent compound $Ca_3Ru_2O_7$, is a member of Ruddlesden-Popper (RP) series perovskite ruthenates $(Sr,Ca)_{n+1}Ru_nO_{3n+1}$ which exhibit a wealth of fascinating physical properties including unconventional superconductivity [28], metamagnetic quantum critical point

[29], and Mott insulators [30]. $Ca_3Ru_2O_7$ crystallizes in an orthorhombic crystal structure with the space group $Bb2_1m$ (No. 36) [31]. It shows an antiferromagnetic transition at T_N = 56 K and a metal-to-insulator transition at T_{MIT} = 48 K [32]. Below T_N, the magnetic moments are ordered in a collinear CM antiferromagnetic structure with spins coupled parallel within the bilayer but antiparallel between adjacent bilayers along the *c* axis. The staggered magnetic moments are aligned along the *b* axis (denoted as AFM-b in Fig. 1(a)) below T_{MIT} and along the *a* axis (denoted as AFM-a) at $T_{MIT} < T < T_N$ [33]. Upon Fe substitution for Ru, $Ca_3(Ru_{1-x}Fe_x)_2O_7$ (x = 0.05) exhibits the coexistence of CM AFM-b type magnetic structure and a cycloidal ICM one below T_{MIT} = 43 K, and an AFM-a type magnetic structure at $T_{MIT} < T < T_N$ (83 K). The ICM component is characterized by nearly temperature-independent wave vectors $\mathbf{q}_{ic}$ = (δ 0 1), δ ~ ±0.017, as shown in Fig. 1(c), and it spontaneously forms a magnetic soliton lattice at zero field as affirmed by the observation of the third-order harmonics of the primary magnetic reflections $\mathbf{q}_{ic}$ in the neutron diffraction measurements [34]. Since the crystal structure of Fe-doped $Ca_3Ru_2O_7$ is noncentrosymmetric ($Bb2_1m$), such a modulated spin structure may be ascribed to the associated Dzyaloshinskii-Moriya (DM) interaction and its competition with the exchange interactions and magnetic anisotropy. The small incommensurability δ indicates a large periodicity of the ICM phase, which is approximately ~ 58 unit cells or ~ 315 Å along the *a* axis [14].

$Ca_3(Ru_{0.95}Fe_{0.05})_2O_7$ single crystals were grown by the floating zone technique. Neutron diffraction experiments were performed using the two-axis diffractometer (E4) in Helmholtz Zentrum Berlin (HZB, Germany) and the triple-axis spectrometer (CTAX) at High Flux Isotope Reactor (HFIR) in Oak Ridge National Laboratory (ORNL, USA). The wavelength of the incident neutron is λ = 2.434 Å at E4, and λ = 4.045 Å was chosen at CTAX in order to get better

resolution in momentum space. The sample was aligned in the horizontal (H 0 L) scattering plane, where H and L are in reciprocal lattice units (r.l.u.) of $2\pi/a \sim 1.17$ Å^{-1} and $2\pi/c \sim 0.32$ Å^{-1}. The vertical magnetic field was applied along the b axis that is perpendicular to the scattering plane. The neutron intensity was presented in the unit of counts per monitor count unit (mcu), with 1 mcu corresponding to approximately ~1 second.

Figures 2(a) and 2(b) show the contour maps of the neutron diffraction intensity of scans along the [1 0 0] direction across the magnetic Bragg peak $\mathbf{q}_c$ = (0 0 1) at T = 15 K after cooling down the sample in zero field (ZFC). The measurement fields are denoted by the light grey grids. At zero field, CM and ICM magnetic peaks are observed at $\mathbf{q}_c$ = (0 0 1) and $\mathbf{q}_{ic}$ = (δ 0 1), $\delta \sim \pm 0.017$, respectively, and there is sizable diffuse scattering intensity centered at the CM (0 0 1) peak, in agreement with the previous report [34]. As the magnetic field increases (Fig. 2(a)), the intensity of the ICM magnetic Bragg peaks at $\mathbf{q}_{ic}$ is suppressed and vanishes in proximity to the critical field $B_{\uparrow}^{c}$ = 4.7 ± 0.1 T. Concomitantly, the CM Bragg peak centered at $\mathbf{q}_c$ gets enhanced and the intensity due to diffuse scattering disappears. This observation clearly indicates a first-order magnetic field-driven ICM-to-CM phase transition with an abrupt change in the magnetic wave vector. Note that the width of these magnetic Bragg peaks is not resolution limited, indicating a correlation length of ~370a for the CM state and ~340a for the ICM phase at zero field, and ~580a for the CM phase at 9 T at T = 1.5 K, where a is the lattice constant. Since the reflection condition due to the symmetry of the crystal structure requires either both H and L are even or the sum of H and L is even, the enhancement in the intensity of (0 0 1) suggests the formation of a magnetic phase at $B > B_{\uparrow}^{c}$. We have measured a series of magnetic Bragg peaks in the reciprocal space at (0 0 3), (0 0 5), (0 0 7), etc. The analysis on the magnetic structure of the field-induced CM phase is very similar to that in the pristine and Ti-doped $Ca_3Ru_2O_7$ [33,35], as

described in detail in the Supplemental Material [36]. The field-induced CM phase above $B_{\uparrow}^{c}$ is determined as a canted antiferromagnetic (CAFM) structure as shown in Fig. 1(b) [36]. Such a field-induced ICM-to-CM transition may arise from the competition among Zeeman energy, exchange energy, and DM interaction [38], a mechanism similar to what was reported in a DM-induced spin spiral $Ba_2CuGe_2O_7$ [39].

Very intriguingly, as the magnetic field decreases, the system cannot restore to its original zero-field state. As shown in Fig. 2(b), the CM CAFM spin structure transforms into the coexistence of CM and ICM ones below the lower critical field $B_{\downarrow}^{c} = 4.3 \pm 0.5$ T, corroborating the first-order character of the field-induced magnetic phase transition. While the CM magnetic Bragg peak is still located at $\mathbf{q}_c = (0\ 0\ 1)$, the ICM ones are centered at $\mathbf{q}_{ic} \sim (\pm 0.005\ 0\ 1)$ in contrast to $(\pm 0.017\ 0\ 1)$ prior to applying the magnetic field. As the magnetic field decreases further down to zero field, this new incommensurability remains unchanged and does not restore to the initial value, i.e., $\mathbf{q}_{ic} \sim (\pm 0.017\ 0\ 1)$.

Figures 2(c) and 2(d) present the line scans measured at $T = 1.5$ K and $B = 0$ T before (denoted as $0_{\uparrow}$ T) and after (denoted as $0_{\downarrow}$ T) ramping the magnetic field up to 9 T. We have observed several remarkable features. (i) In addition to the primary (first-order) ICM magnetic reflections (marked by green arrows) discussed above, the third-order harmonic peaks (marked by orange arrows) are also observed for both $0_{\uparrow}$ T and $0_{\downarrow}$ T states. This feature suggests that the magnetic soliton lattice reemerges at the $0_{\downarrow}$ T state, but with a much longer periodicity at $0_{\downarrow}$ T state (~200 unit cells or ~1100 Å along the *a* axis). (ii) The intensity ratio of the third- to the first-order harmonic peaks I_3/I_1 is much larger at $B = 0_{\downarrow}$ T, suggesting that the associated ICM magnetic structure is more distorted from the uniform cycloidal structure with narrower domain wall width. (iii) While the full width at half maximum (FWHM) of the CM peak remains nearly

unchanged compared to the one at the $0_{\uparrow}$ T state, the FWHM of the ICM magnetic peaks at the $0_{\downarrow}$ T state becomes broader, implying a shorter correlation length of the soliton lattice at the $0_{\downarrow}$ T state. It is worth noting that such a $0_{\downarrow}$ T phase is rather persistent and subsequent magnetic field cycling between 0 T and 9 T shows a reversible behavior with the magnetic wave vector changing between ICM $\mathbf{q}_{ic} \sim (\pm 0.005\ 0\ 1)$ and CM $\mathbf{q}_c = (0\ 0\ 1)$, unless the temperature is raised high enough (more discussions later). These results suggest that the system could not restore to its equilibrium ground state after the field-induced ICM-to-CM phase transition. Instead, it forms a persistent metastable state at low temperature, leading to an irreversible behavior of the modulation wave vector in the field-induced magnetic phase transition [36].

Figures 3(a)-3(c) present the irreversibility of the field-driven ICM-CM magnetic structure transition at representative temperatures. The neutron diffraction scans along the [1 0 0] direction were performed at zero field under two different histories following the aforementioned procedure, one right after ZFC to the designated temperature ($0_{\uparrow}$ T, black curve) and the other after ZFC and applying the magnetic field up to 9 T then removing the magnetic field ($0_{\downarrow}$ T, red curve). One can see that the wave vector of the primary ICM magnetic reflection $\mathbf{q}_{ic}$ in the $0_{\uparrow}$ T state stays almost constant below T_{MIT}, consistent with the previous report [34]. However, the $0_{\downarrow}$ T state behaves in a completely different way with $\mathbf{q}_{ic}$ of the ICM Bragg peak depending on the measurement temperature. A summary of the zero-field incommensurability δ measured at both $0_{\uparrow}$ T and $0_{\downarrow}$T states is presented in Fig. 3(d). In contrast to the constant $\delta \sim \pm 0.017$ at the $0_{\uparrow}$ T state, δ at the $0_{\downarrow}$T state is relatively smaller and remain unchanged below 18 K, above which δ increases monotonically and gradually reaches the value of the equilibrium state $\sim \pm 0.017$. This indicates that a complete recovery of the original equilibrium ground state at the $0_{\downarrow}$T state takes place at a characteristic temperature $T_g \sim 37$ K that is slightly lower than T_{MIT}. In addition, it is

noteworthy that the ICM peaks in the $0_{\downarrow}$T state, for example at 20 K (Fig. 3(a)), are much broader than that of the equilibrium $0_{\uparrow}$ T phase, suggesting a shorter correlation in the ICM structures in the $0_{\downarrow}$T state (~230a in the $0_{\downarrow}$ T phase and ~340a in the $0_{\uparrow}$ state, with fitting scheme described in detail in the Supplemental Material [36]). These features suggest that the emergence of the field-induced metastable state $0_{\downarrow}$T at low temperature is due to the fact that the system gets trapped at a local minimum in the free energy landscape. As a result, the transformation to the equilibrium ground state ($0_{\uparrow}$ T) is kinetically prohibited by the energy barriers unless the thermal fluctuation is strong enough to overcome this barrier.

To further understand the temperature evolution of the field-induced metastable state ($0_{\downarrow}$T), we prepared the initial $0_{\downarrow}$ T state at T = 1.5 K and then performed the measurements at various temperatures while gradually warming up the sample. The data are shown in Fig. 4(a) (2K/step, as indicated by the light grey grids). One can see that the ICM wave vector $\mathbf{q}_{ic}$ ~ (±0.005 0 0) remains almost unchanged until T ~ 31 K and then starts to evolve gradually towards the equilibrium ground state with $\mathbf{q}_{ic}$ ~ (±0.017 0 1) which is eventually realized at T_g ~ 37 K. In the meantime, the intensity at the CM (0 0 1) gets much weaker and the peak width becomes narrower, due to the increasing fraction of the ICM phase when transforming from the metastable state to the equilibrium one. Notably, the temperature where $\mathbf{q}_{ic}$ starts to deviate from that of the low-temperature $0_{\downarrow}$ T state is sensitively dependent on the measurement procedures, as shown in Fig. 3(d) and Fig. 4(a), i.e., the former at T ~ 18 K and the latter at T ~ 31 K, indicating that the incommensurability of the $0_{\downarrow}$ T state obtained using different measurement protocols can be quite different for 18 K < T < 31 K. This implies that a mechanism, which is sensitively dependent on both temperature and magnetic field history, has to be invoked in order to explain this irreversible behavior. Figure 4(b) shows the evolution of the third-order harmonics measured

at $0_{\downarrow}$T at representative temperatures. The temperature dependence of the intensity ratio I_3/I_1 is shown in the inset. As the temperature increases, the intensity ratio I_3/I_1 decreases, indicating that the ICM magnetic soliton lattice gradually evolves towards the uniform cycloidal spin structure with broader domain wall width at elevated temperatures, similar to the zero-field study reported previously [34].

The observation of ICM magnetic structures with irreversible modulation wave vectors in the field-induced ICM-CM magnetic transitions in Fe-doped $Ca_3Ru_2O_7$ is quite intriguing. One may be tempted to attribute the irreversibility to the coupling between the CM AFM-b structures and the ICM magnetic structures since they coexist in this material. However, such a scenario may not be valid since no convincing evidence that suggests any correlation between the intensity, correlation length or the diffuse intensity of the commensurate peak and the modulation wave vector $\mathbf{q}_{ic}$ is seen in the neutron diffraction experiment [36]. Interestingly, similar irreversible behavior in the modulation wave vector has been reported in the pressure dependence of the spin density wave in metallic Cr [24], and the field dependence of magnetic structure in the multiferroic $TbMnO_3$ [25], $DyMn_2O_5$ [26] and the *f*-electron system UNiAl [27]. In spite of the absence of a unifying microscopic theory to address such irreversibility, the phenomenological theories proposed to account for the metastability in Cr [40,41] may shed light on the underlying mechanism of the observation in our study. First, spin-lattice coupling. It was suggested that the lattice distortions induced by the spin density wave ordering has negative free energy, which results in the persistence of the domain walls when ramping down the pressure and leads to the metastability in the modulation wave vector [40]. However, this is not likely the origin of the metastability observed in Fe-doped $Ca_3Ru_2O_7$, since there is no noticeable change in the lattice constants at the field-induced transition. In addition, no lattice modulation peaks at

$2\mathbf{q}_{ic}$ displaced from the nuclear peak (0 0 4) is convincingly observed in Fe-doped $Ca_3Ru_2O_7$, as shown in Fig. S6 [36], in contrast to that in Cr which indicates the presence of strong exchange striction [42]. Second, domain wall pinning. It was proposed that the metastability in the modulation wave vector in Cr can also stem from the pinning of domain walls to nonmagnetic impurities [41]. However, rather than the nonmagnetic impurities which presumably interact weakly with the magnetic domain walls and has minimum pinning effect [43], it is more likely that the interaction between magnetic Fe dopants and domain walls is responsible for the metastability in the ordering wave vector in Fe-doped $Ca_3Ru_2O_7$. We suggest that although these randomly doped magnetic impurities can enhance the heterogeneous nucleation process of the magnetic domain walls during the CM-to-ICM transition when the magnetic field ramps down, they also pin the domain walls and thus create energy barriers and prevent the domain wall density from reaching the equilibrium value, leading to the observed metastability [41].

To summarize, we have studied the irreversible behaviors in the modulation wave vector of $Ca_3(Ru_{1-x}Fe_x)_2O_7$ (x = 0.05) in a field-induced first-order ICM-CM phase transition. At low temperature, the incommensurability of the metastable magnetic soliton lattice at zero field is sensitively dependent on the magnetic field and temperature history. The metastable state evolves towards the equilibrium state as temperature increases up to $T_g \sim 37$ K. Such metastability in the modulation wave vector is presumably attributed to domain wall pinning by the magnetic Fe dopants. Therefore, the bilayer ruthenate Fe-doped $Ca_3Ru_2O_7$ provides an ideal material system to study the metastability problem of the magnetic soliton lattice phase, which deserves further theoretical investigation.

The work at Michigan State University was supported by the National Science Foundation under Award No. DMR-1608752 and the start-up funds from Michigan State

University. The work at Tulane is supported by the U.S. Department of Energy under EPSCoR Grant No. DE-SC0012432 with additional support from the Louisiana Board of Regents and work at ORNL was supported by the Scientific User Facilities Division, Office of Basic Energy Sciences, DOE. Work at Nanjing University was supported by the National Natural Science Foundation of China (No. 11304149). We thank HZB for the allocation of neutron beamtime.

Figure Captions

Figure 1. Schematic diagrams of the crystal and magnetic structures of $Ca_3(Ru_{0.95}Fe_{0.05})_2O_7$. The blue arrow represents the direction of the magnetic field. (a) AFM-b: ferromagnetic bilayers stacked antiferromagnetically along the *c* axis. (b) CAFM: canted antiferromagnetic structure induced by a magnetic field along the *b* axis. (c) In-plane view of the magnetic structure at $T < T_{MIT}$ at $B = 0$ T. It has a CM component of AFM-b type (denoted as CM(AFM-b)) and an ICM one forming a magnetic soliton lattice that propagates along the *a* axis (ICM (soliton lattice)). The square in magenta denotes one unit cell and the rounded rectangle in orange highlights the domain wall (soliton).

Figure 2. (a), (b) Contour maps of the neutron diffraction intensity of scans along [1 0 0] direction across the magnetic wave vector $\mathbf{q}_c = (0\ 0\ 1)$ in a magnetic field along the *b* axis at $T =$ 15 K. The light grey girds denote the measurement field. (c), (d) Neutron diffraction scans along the [1 0 0] direction across the magnetic Bragg peak $\mathbf{q}_c = (0\ 0\ 1)$ in the $0_{\uparrow}$ and $0_{\downarrow}$T phases (defined in the text) at 1.5 K, respectively. The dark green and orange arrows mark the wave vector of the first-order ICM magnetic Bragg peaks and their third-order harmonics, respectively, while the purple ones mark the CM reflections. Inset shows the zoom-in view of the third-order harmonics at $T = 1.5$ K and 80 K, respectively, for $B = 0_{\uparrow}$ T. The data were taken at CTAX.

Figure 3. (a)-(c) Neutron diffraction scans along [1 0 0] direction across the wave vector $\mathbf{q}_c = (0\ 0\ 1)$ in the $0_{\uparrow}$ and $0_{\downarrow}$T phases (defined in the text) at representative temperatures. The Bragg peaks have been fitted using Gaussian functions (solid curves). An additional Gaussian function was used for $T = 20$ K data to account for the broad feature centered at (0 0 1). The grey horizontal line indicates the instrument resolution. (d) Incommensurability δ of the primary ICM magnetic wave vector $\mathbf{q}_{ic} = (\delta\ 0\ 1)$ in the $0_{\uparrow}$ and $0_{\downarrow}$T phases at different temperatures. The error

bars obtained from Gaussian fitting are smaller than the symbol size. The solid curves are guide to the eye. The data were taken at CTAX.

Figure 4. (a) Contour map of the neutron diffraction intensity of scans along [1 0 0] direction over $\mathbf{q_c}$ = (0 0 1) while warming up in the metastable $0_{\downarrow}$T phase. The measurement fields are denoted by the light grey grids. (b) Neutron diffraction scans along [1 0 0] direction over $\mathbf{q_c}$ = (0 0 1) at representative temperatures. The third-order harmonics of the ICM magnetic reflections are denoted by orange arrows. Inset shows the temperature dependence of the intensity ratio I_3/I_1 in the $0_{\downarrow}$ phase. Note that the measurement procedures of the data shown in Fig. 3 and 4 are different, as described in the text. The data were taken at CTAX.

Figure 1

M. Zhu *et al*.

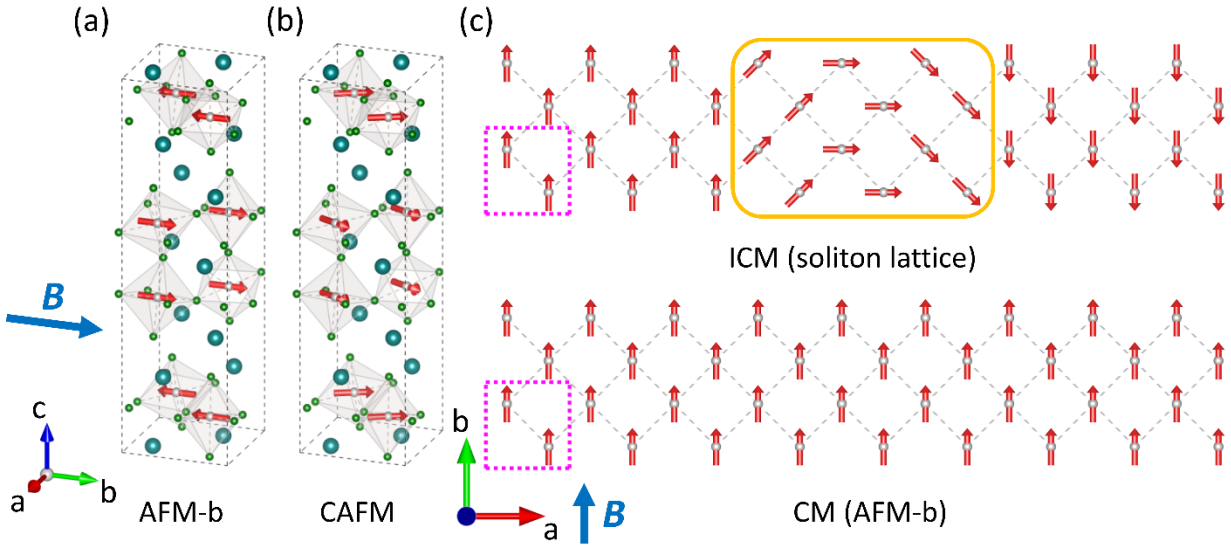

Figure 2

M. Zhu *et al*.

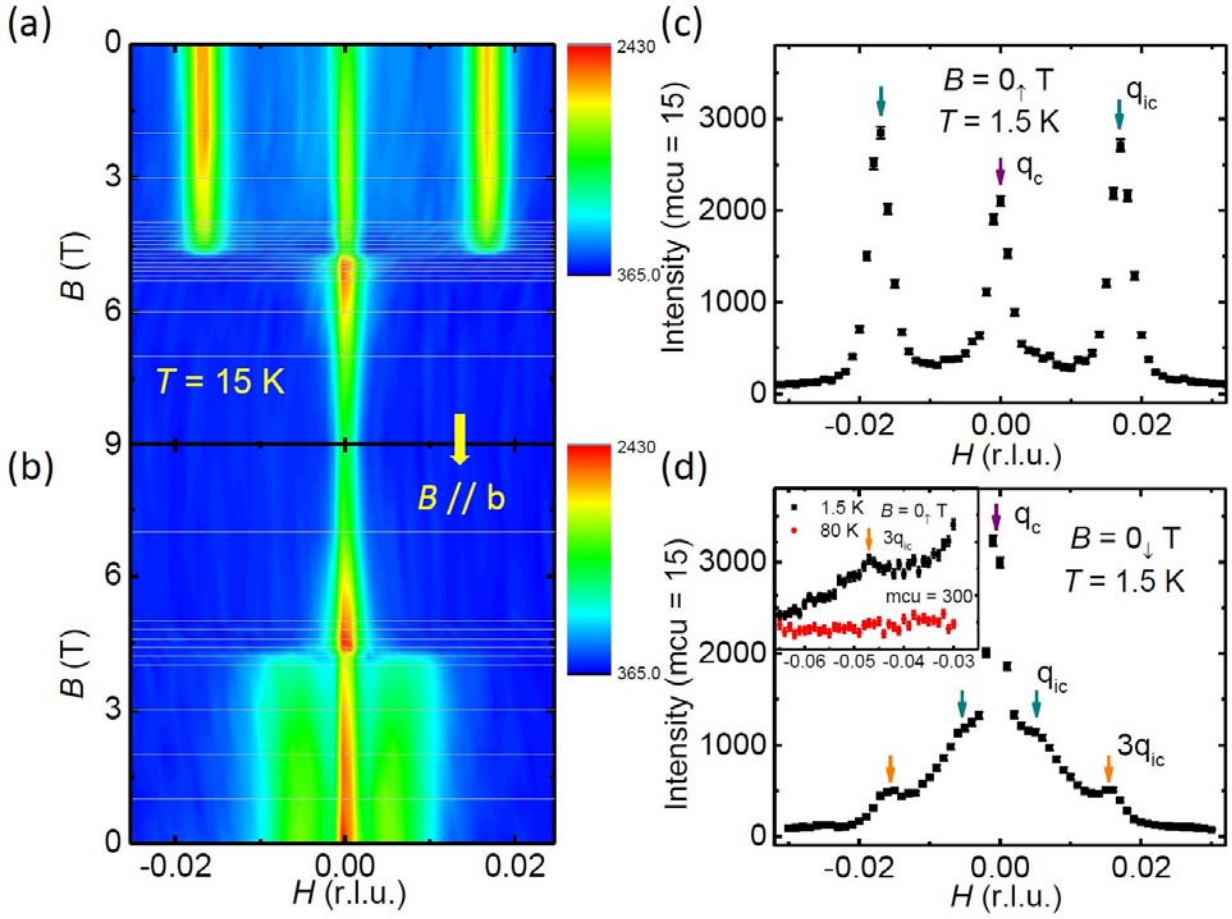

Figure 3

M. Zhu *et al*.

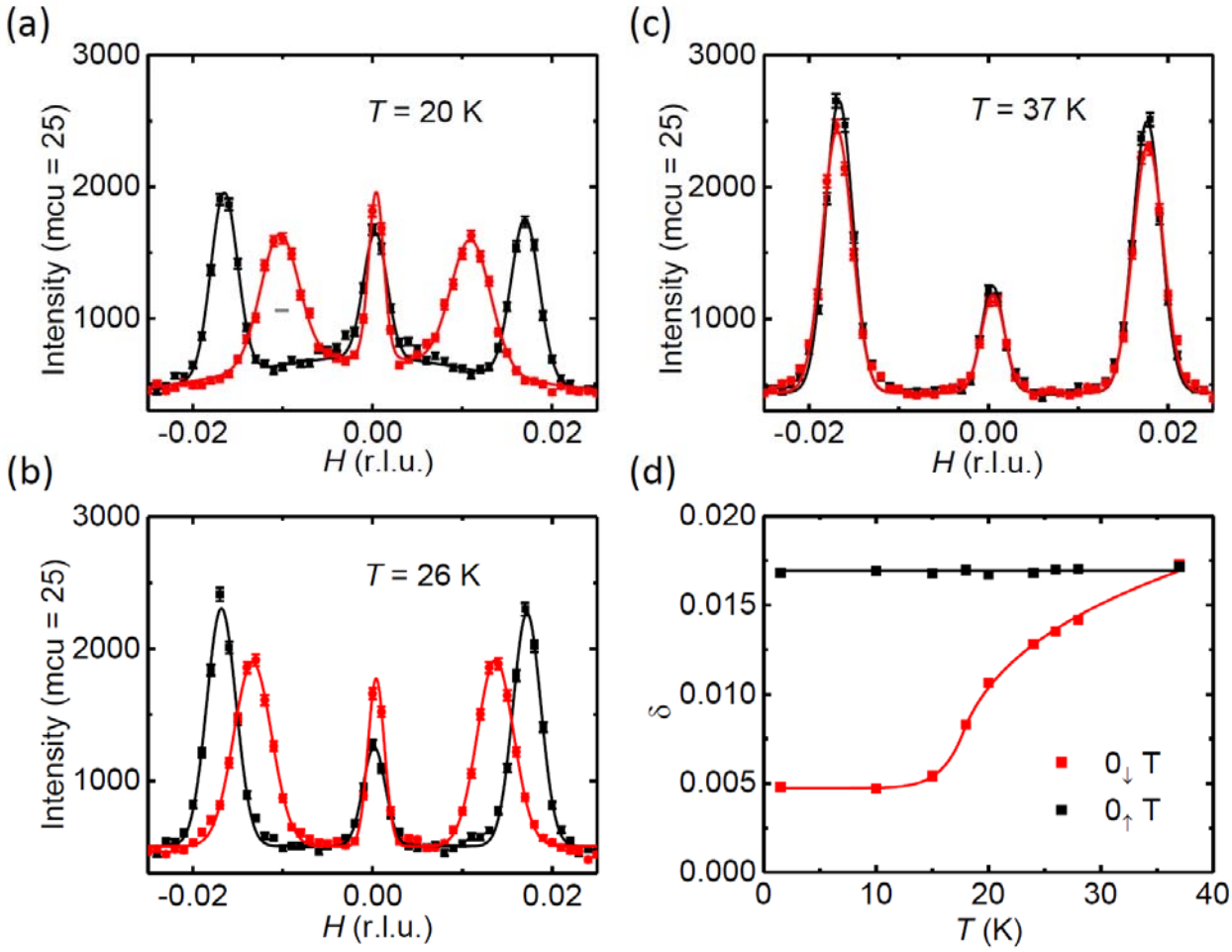

Figure 4

M. Zhu *et al*.

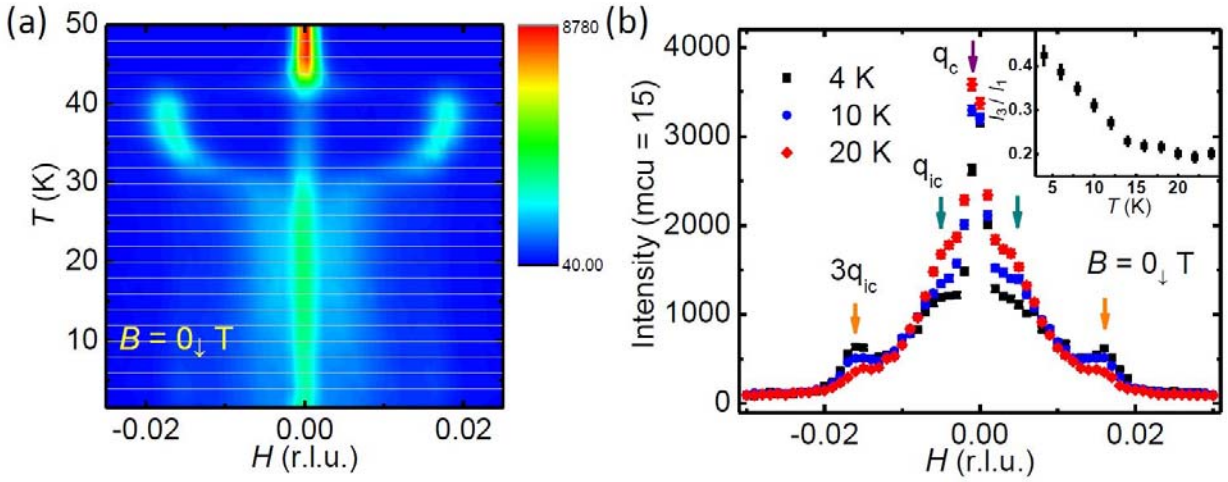

[1] L. D. Landau and E. M. Lifshitz, Physical Kinetics **vol. 10 of Course of Theoretical Physics**, p. 427 (1981).
[2] Pablo G. Debenedetti and Frank H. Stillinger, Nature **410** (6825), 259 (2001).
[3] H. Kuwahara, Y. Tomioka, A. Asamitsu, Y. Moritomo, and Y. Tokura, Science **270** (5238), 961 (1995).
[4] Y. Tomioka, A. Asamitsu, H. Kuwahara, Y. Moritomo, and Y. Tokura, Physical Review B **53** (4), R1689 (1996).
[5] R. Rawat, K. Mukherjee, Kumar Kranti, A. Banerjee, and P. Chaddah, Journal of Physics: Condensed Matter **19** (25), 256211 (2007).
[6] Kranti Kumar, A. K. Pramanik, A. Banerjee, P. Chaddah, S. B. Roy, S. Park, C. L. Zhang, and S. W. Cheong, Physical Review B **73** (18), 184435 (2006).
[7] P. Das, C. Rastovski, T. R. O'Brien, K. J. Schlesinger, C. D. Dewhurst, L. DeBeer-Schmitt, N. D. Zhigadlo, J. Karpinski, and M. R. Eskildsen, Phys Rev Lett **108** (16), 167001 (2012).
[8] C. Rastovski, K. J. Schlesinger, W. J. Gannon, C. D. Dewhurst, L. DeBeer-Schmitt, N. D. Zhigadlo, J. Karpinski, and M. R. Eskildsen, Phys Rev Lett **111** (10), 107002 (2013).
[9] R. M. Fleming, D. E. Moncton, and D. B. McWhan, Physical Review B **18** (10), 5560 (1978).
[10] Katsumi Hamano, Kenji Ema, and Shunsuke Hirotsu, Ferroelectrics **36** (1), 343 (1981).
[11] P. Prelovšek, Phase Transitions **11** (1-4), 203 (1988).
[12] Sang-Wook Cheong and Maxim Mostovoy, Nature materials **6** (1), 13 (2007).
[13] Tsuyoshi Kimura, Annual Review of Condensed Matter Physics **3** (1), 93 (2012).
[14] Yu. A. Izyumov, Soviet Physics Uspekhi **27** (11), 845 (1984).
[15] R. A. Cowley and S. Bates, Journal of Physics C: Solid State Physics **21** (22), 4113 (1988).
[16] M. Habenschuss, C. Stassis, S. K. Sinha, H. W. Deckman, and F. H. Spedding, Physical Review B **10** (3), 1020 (1974).
[17] B. Roessli, J. Schefer, G. A. Petrakovskii, B. Ouladdiaf, M. Boehm, U. Staub, A. Vorotinov, and L. Bezmaternikh, Physical Review Letters **86** (9), 1885 (2001).
[18] A. Zheludev, S. Maslov, G. Shirane, Y. Sasago, N. Koide, and K. Uchinokura, Physical Review Letters **78** (25), 4857 (1997).
[19] S. Artyukhin, M. Mostovoy, N. P. Jensen, D. Le, K. Prokes, V. G. de Paula, H. N. Bordallo, A. Maljuk, S. Landsgesell, H. Ryll, B. Klemke, S. Paeckel, K. Kiefer, K. Lefmann, L. T. Kuhn, and D. N. Argyriou, Nature materials **11** (8), 694 (2012).
[20] Y. Togawa, T. Koyama, K. Takayanagi, S. Mori, Y. Kousaka, J. Akimitsu, S. Nishihara, K. Inoue, A. S. Ovchinnikov, and J. Kishine, Physical Review Letters **108** (10), 107202 (2012).
[21] Y. Togawa, T. Koyama, Y. Nishimori, Y. Matsumoto, S. McVitie, D. McGrouther, R. L. Stamps, Y. Kousaka, J. Akimitsu, S. Nishihara, K. Inoue, I. G. Bostrem, Vl E. Sinitsyn, A. S. Ovchinnikov, and J. Kishine, Physical Review B **92** (22), 220412(R) (2015).
[22] Hak Bong Lee, Young-Sang Song, Jae-Ho Chung, Sae Hwan Chun, Yi Sheng Chai, Kee Hoon Kim, M. Reehuis, K. Prokeš, and S. Mat'aš, Physical Review B **83** (14), 144425 (2011).
[23] S. Holbein, M. Ackermann, L. Chapon, P. Steffens, A. Gukasov, A. Sazonov, O. Breunig, Y. Sanders, P. Becker, L. Bohatý, T. Lorenz, and M. Braden, Physical Review B **94** (10), 104423 (2016).

[24] D. W. Ruesink, J. M. Perz, and I. M. Templeton, Physical Review Letters **45** (9), 734 (1980).
[25] D. Senff, P. Link, N. Aliouane, D. N. Argyriou, and M. Braden, Physical Review B **77** (17), 174419 (2008).
[26] W. Ratcliff, V. Kiryukhin, M. Kenzelmann, S. H. Lee, R. Erwin, J. Schefer, N. Hur, S. Park, and S. W. Cheong, Physical Review B **72** (6), 060407 (2005).
[27] K. Prokeš, F. Bourdarot, P. Burlet, M. Olšovec, V. Sechovský, P. Javorský, E. Brück, A. Goukassov, F. R. de Boer, and A. A. Menovsky, Physica B: Condensed Matter **259–261**, 246 (1999).
[28] Andrew Peter Mackenzie and Yoshiteru Maeno, Reviews of Modern Physics **75** (2), 657 (2003).
[29] S. A. Grigera, R. S. Perry, A. J. Schofield, M. Chiao, S. R. Julian, G. G. Lonzarich, S. I. Ikeda, Y. Maeno, A. J. Millis, and A. P. Mackenzie, Science **294** (5541), 329 (2001).
[30] S. Nakatsuji and Y. Maeno, Physical Review Letters **84** (12), 2666 (2000).
[31] Yoshiyuki Yoshida, Shin-Ichi Ikeda, Hirofumi Matsuhata, Naoki Shirakawa, C. H. Lee, and Susumu Katano, Physical Review B **72** (5), 054412 (2005).
[32] G. Cao, S. McCall, J. E. Crow, and R. P. Guertin, Physical Review Letters **78** (9), 1751 (1997).
[33] Wei Bao, Z. Q. Mao, Z. Qu, and J. W. Lynn, Physical Review Letters **100** (24), 247203 (2008).
[34] X. Ke, J. Peng, W. Tian, Tao Hong, M. Zhu, and Z. Q. Mao, Physical Review B **89** (22), 220407 (2014).
[35] M. Zhu, J. Peng, T. Zou, K. Prokes, S.□D. Mahanti, T. Hong, Z. Q. Mao, G.□Q. Liu, and X. Ke, Physical Review Letters **116** (21), 216401 (2016).
[36] See Supplemental Material, which includes Ref. [37] for the magnetic phase diagram when the field increases, the determination on the CAFM structure and the discussions on the equilibrium state.
[37] Juan Rodríguez-Carvajal, Physica B: Condensed Matter **192** (1–2), 55 (1993).
[38] A. N. Bogdanov, A. V. Zhuravlev, and U. K. Rößler, Physical Review B **75** (9), 094425 (2007).
[39] A. Zheludev, S. Maslov, G. Shirane, Y. Sasago, N. Koide, and K. Uchinokura, Physical Review B **57** (5), 2968 (1998).
[40] E. W. Fenton, Physical Review Letters **45** (9), 736 (1980).
[41] P. B. Littlewood and T. M. Rice, Physical Review Letters **48** (1), 44 (1982).
[42] Y. Tsunoda, M. Mori, N. Kunitomi, Y. Teraoka, and J. Kanamori, Solid State Communications **14** (3), 287 (1974).
[43] I. Tüttö and A. Zawadowski, Physical Review Letters **60** (14), 1442 (1988).